# A Comparison Study of Gabor and Log-Gabor Wavelets for Texture Segmentation

Rodrigo Nava
Posgrado en Ciencia e Ingeniería de la Computación
Universidad Nacional Autónoma de México
Cd. Universitaria, Mexico City, Mexico
Email: urielrnv@uxmcc2.iimas.unam.mx

Boris Escalante-Ramírez
Facultad de Ingeniería
Universidad Nacional Autónoma de México
Cd. Universitaria, Mexico City, Mexico
Email: boris@servidor.unam.mx

Gabriel Cristóbal
Instituto de Óptica
Consejo Superior de Investigaciones Científicas (CSIC)
Serrano 121, Madrid 28006, Spain
Email: gabriel@optica.csic.es

***Abstract*—Texture analysis is a significant challenge for computer vision but not yet solved. Since image textures possess spatial continuity at both local and global scales, they are widely used to perform tasks such as object segmentation or surface analysis. Based on the fact that the human visual system (HVS) can segment textures robustly, many texture segmentation schemes use biological models. Modern theories about the functioning of the HVS lead us think that the visual process takes advantage of image redundancy at different scales and orientations, therefore it can be modeled by a bank of Gabor wavelets. Despite the fact that Gabor wavelets optimize the theoretical limit of joint resolution between space and frequency domain, they do not have zero-mean, which induces a DC component in the coefficient of any frequency band. In addition, they do not have a uniform coverage of the frequency domain. These drawbacks may cause errors in the extraction of the appropriate texture features. In this paper, we present a modification of log-Gabor wavelets that allows eliminate DC component. They can yield a fairly uniform coverage of the frequency domain in an octave scale scheme and preserve redundancy at the same time. We analyzed performance of both Gabor and log-Gabor wavelets using a modification of Jain's unsupervised texture segmentation algorithm [1] and we compared results using confusion matrices.**

## I. Introduction

In recent years, image processing algorithms based on biological models have increased due to greater knowledge of the HVS. The need for the visual system to process efficiently a large amount of information requires that image structures can be extracted and represented in an optimal way. Although we do not know much about the early stages of the visual information process, there is convincing evidence that HVS takes advantage of image redundancy at different scales and orientations [2]. Furthermore, receptive fields of simple cortical cells have strong orientation selectivity [3]. As a result, receptive fields were captured in a model proposed by Denis Gabor [4]. Gabor showed how to represent time-varying signals in terms of functions that are localized in both time and frequency. These functions, described by the product of a Gaussian and a sinusoid, constitute a unique family of linear filters that behave optimally under the uncertainty principle, in the sense that their simultaneous resolution in the two domains is maximal. Moreover, Gabor wavelets do not constitute an orthogonal basis, the number of coefficients in the transform domain is larger than the number of pixels in the image domain introducing redundant information which can be used for improving feature extraction.

The motivation of this paper is to investigate the advantages of log-Gabor wavelet transform and comparing its performance with classical Gabor wavelet transform. In section II we present the Gabor wavelet paradigm and its limitations. Section III describes log-Gabor wavelet transform in details summarizing its properties. In Section IV we propose a modification of Jain's unsupervised texture segmentation algorithm in order to evaluate the performance between Gabor and log-Gabor wavelets. Finally, assessment of results and conclusions are drawn in Section VI.

## II. Gabor wavelets

Daugman [5] proposed an extension of Gabor wavelets because simple receptive fields are deployed in two dimensions and showed that they occupy an irreducible volume in the four-dimensional (4D) hyperspace where four orthogonal axes correspond to the spatial $(x, y)$ and spatial-frequency $(u, v)$ variables. This generalization achieves lower limit of uncertainty relation according with the Information Theory. In addition, properties of 2D Gabor wavelets match the early psychophysical and physiological features of simple cells in human beings and cats [6].

A canonical 2D Gabor wavelet in spatial domain is defined as:

$$g(x,y) = e^{-\pi\left[\alpha^2(x-x_0)^2+\beta^2(y-y_0)^2\right]+2\pi i[u_0(x-x_0)+v_0(y-y_0)+\phi]} \tag{1}$$

where $(x_0, y_0)$ are the center of the filter, $(u_0, v_0)$ and $\phi$ represent the radial frequency and the phase of the sinusoidal signal respectively. $(\alpha, \beta)$ are the space constants of the Gaussian envelope along $x$ and $y$ axes respectively and they control the wavelet bandwidth.

In this paper we used a 2D Gabor wavelet centered at the origin. Only the real part (even part) is considered because filters are in quadrature phase. This fact provides a suitable symmetric filters for detecting salient edges in the images [7].

By applying previous considerations, we obtain the next expression:

$$g(x,y) = e^{-\pi\left(\alpha^2 x^2 + \beta^2 y^2\right)} \cos\left(2\pi u_0 x\right) \tag{2}$$

note that if both even and odd parts of Gabor wavelet are used, they closely approximate to a Hilbert Transform pair [8].

Traditionally, 2D Gabor wavelets are presented in polar coordinates in order to take advantage of their directionality. Taking the rotation matrix (3) and applying in (2) we obtain a 2D polar Gabor representation in (4) as follows:

$$R = \begin{pmatrix} \cos\theta & \sin\theta \\ -\sin\theta & \cos\theta \end{pmatrix} \tag{3}$$

$$g(x,y,) = e^{-\pi\left(\alpha^2 \tilde{x}^2 + \beta^2 \tilde{y}^2\right)} \cos\left(2\pi u_0 \tilde{x}\right) \tag{4}$$

with

$$\begin{aligned} \tilde{x} &= x\cos\theta + y\cos\theta \\ \tilde{y} &= -x\sin\theta + y\cos\theta \end{aligned} \tag{5}$$

where $\theta$ denotes the rotation angle of both Gaussian and plane wave. Equation (4) has been used in texture analysis successively as described in [9], [10].

The frequency and orientation selective properties of Gabor wavelets can be more explicit in Fourier domain. The Fourier transform of $g$ is

$$\begin{aligned} G(u,v) &= e^{-\pi\left[\frac{(\tilde{u}-u_0\cos\theta)^2}{\alpha^2} + \frac{(\tilde{v}+u_0\sin\theta)^2}{\beta^2}\right]} \\ &+ e^{-\pi\left[\frac{(\tilde{u}+u_0\cos\theta)^2}{\alpha^2} + \frac{(\tilde{v}+u_0\sin\theta)^2}{\beta^2}\right]} \end{aligned} \tag{6}$$

where $(\tilde{u},\tilde{v}) = (u\cos\theta + v\sin\theta, -u\sin\theta + v\cos\theta)$.

$G(u,v)$ represents a Gaussian with $u$ frequency units shifted along $u$ axis and counterclockwise rotated by an angle $\theta$.

Selection of optimal Gabor parameters has been an issue and depends on the application problem. There are many possibilities, one of them is to experiment with the width of the Gaussian envelope by changing $(\alpha,\beta)$ values, which determine the resolution in both spatial and frequency domains. Thus, $G(u,v)$ is a band pass filter with bandwidth controlled by $\alpha$ and $\beta$. If aspect ratio $\lambda = \frac{\alpha}{\beta} = 1$ then (6) is an isotropic filter. The main problem lies in choosing radial frequency $u$ that defines the degree of overlapping between two adjacent filters. The higher the central frequency of the Gabor sinusoidal carrier, the smaller area the Gaussian envelope will cover in the spatial domain [11]. By changing values of radial frequency $u$ and orientation $\theta$ is possible to cosntruct a filter bank as it is shown in Figure 1.

### A. Limitations

Gabor wavelets possess a number of interesting mathematical properties: first, they have a smooth and indefinitely differentiable shape. Second, they do not have side lobes neither in space nor frequency domain. Nevertheless, Gabor wavelets present some important drawbacks which we review in the next list.

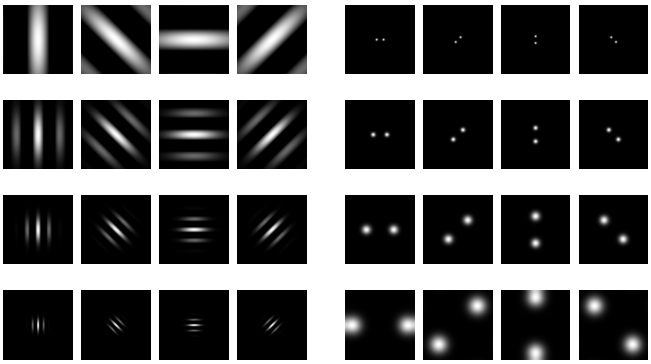

(a) (b)

Figure 1. Gabor wavelet filter bank with 4 scales, where radial frequency $u = \left\{8\sqrt{2}, 16\sqrt{2}, 32\sqrt{2}, 64\sqrt{2}\right\}$ is defined in cycles/image-width, and 4 orientations $\theta = \left\{0, \frac{\pi}{4}, \frac{\pi}{2}, \frac{3\pi}{4}\right\}$. (a) Real part in spatial domain. (b) Gabor wavelets in Fourier domain.

In [12], Fischer points out that there are three main drawbacks of Gabor wavelets which have complicated their usage:

- The filter averaging is not null and therefore the DC component influences intermediate bands. Filters overlap at low frequencies more than in higher ones yielding a non-uniform coverage of the Fourier domain, (see Figure 2).
- The traditional arrangement in scales and orientations of filters does not cover uniformly the Fourier plane and therefore the reconstruction is not exact. In fact, Gabor wavelets are bandpass filters by definition, and then they can not cover lowest and highest frequencies.
- It is not possible to build a complete orthogonal basis of Gabor functions. Non-orthogonality implies that exact reconstruction using the same filters for analysis and synthesis will not be possible unless an overcomplete dictionary is considered [7].

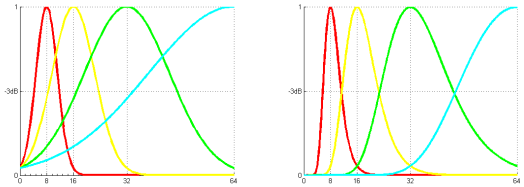

(a) (b)

Figure 2. Profiles of the frequency response of (a) Gabor wavelets and (b) log-Gabor wavelets. Note that DC component is minimized by introducing log (natural logarithm)function and the frequency bands become more disjointed as well.

## III. Log-Gabor wavelets

Log-Gabor wavelets, firstly proposed by D. Field [3], are defined in the frequency domain due to the singularity in the log function at origin. They always have a null DC component and can be optimized to produce filters with minimal spatial extent. They can be divided into two components: radial and

angular filters $G(\rho,\theta) = G_\rho G_\theta$ as in Figure 3.

$$G(\rho,\theta) = e^{-\frac{\log^2\left(\frac{\rho}{u_0}\right)}{2\log^2\left(\frac{\sigma_\rho}{u_0}\right)}} e^{-\frac{(\theta-\theta_0)^2}{2\sigma_\theta^2}} \tag{7}$$

where $(\rho,\theta)$ represents the polar coordinates, $u_0$ is the center frequency, $\theta_0$ is the orientation angle, $\sigma_\rho$ determines the scale bandwidth and $\sigma_\theta$ determines the angular bandwidth [13].

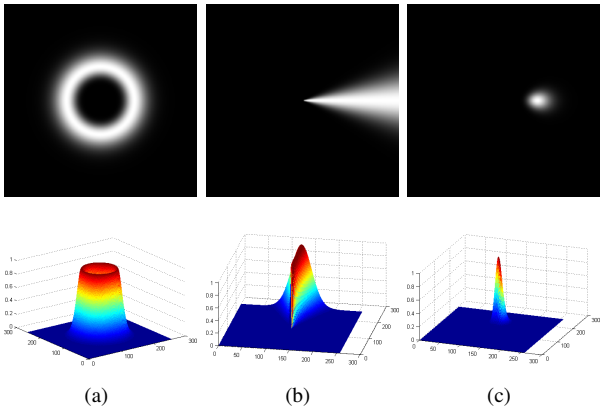

(a) (b) (c)

Figure 3. An example of the log-Gabor filter with $u_0 = 64\sqrt{2}$, $\theta_0 = 0°$, $\sigma_\rho = 0.8$, and $\sigma_\theta = \frac{\pi}{8}$. (a) Radial component of the filter. (b) Angular component of the filter. (c) Product of the two components to produce the representation of the log-Gabor filter in the frequency domain.

In this paper we followed the new design of log-Gabor wavelets proposed in [12]. Fischer's model improves Field's model and allows exact reconstruction by a self-invertible transform (the same transform functions are used for the direct and invert transform). The proposed model lacks DC component and can yield a fairly uniform coverage of the frequency domain in an octave scale scheme.

$$G_{s,l}(\rho,\theta) = e^{-\frac{(\rho-\rho_s)^2}{2\sigma_\rho^2}} e^{-\frac{\left(\theta-\theta_{(s,l)}\right)^2}{2\sigma_\theta^2}} \tag{8}$$

where $(\rho,\theta)$ are the log-polar coordinates and $(\sigma_\rho,\sigma_\theta)$ are the angular and radial bandwidths (common for all the filters). The pair $\left(\rho_s,\theta_{(s,l)}\right)$ corresponds to the frequency center of the filter. In addition, the scheme is completed by a Gaussian low-pass filter. Further filtering parameters were tuned by following the design constraints recommended in [12].

One of its particularities is that even scales are rotated by a constant factor consisting of the half distance between filter centers, (see Figure 4), in order to better cover the Fourier plane.

## IV. Texture Segmentation

Numerous methods for texture segmentation based on Gabor filters have been proposed in the literature [8], [10]. In order to compare both Gabor and log-Gabor schemes we selected an unsupervised algorithm proposed by Jain and Farrokhnia [1]. In the rest of this section we present our implementation and the main differences in relation with the Jain's method. Figure 5 shows a block diagram of this algorithm.

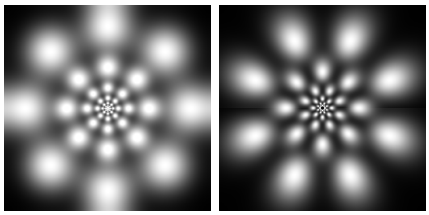

(a) (b)

Figure 4. Multiscale (a) Gabor and (b) log-Gabor arrangements with 4 orientations and 6 scales. Note that log-Gabor scheme shows even scales rotated a half distance between filter centers.

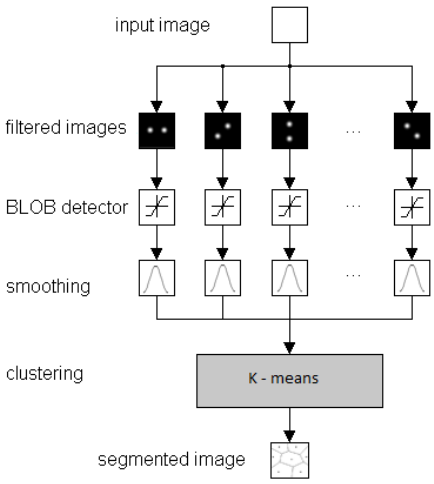


Figure 5. Block diagram for unsupervised texture segmentation algorithm, originally proposed by Jain and Farrokhnia in [1]. After the decomposition of the image using Gabor wavelets, the coefficients obtained are filtered by a nonlinear transformation. This process generates features which are classified by a K-means algorithm.

### A. Setting Gabor filter bank parameters

Jain proposed to use 28 real Gabor filters (4 orientations and 7 scales) for the texture segmentation and the tests were performed using images of size $256 \times 256$.

Based on the studies of Bovik in [8] we decided to change the filter settings, e.g. the frequency and angular bandwidths $(B_u, B_\theta)$ can be set to constant values to match psychovisual data. We used the next equation in order to determine $\alpha$ value in equation (6):

$$\alpha = \frac{\sqrt{\log(2)}\left(2^{B_u}+1\right)}{\sqrt{2}\pi u\left(2^{B_u}-1\right)} \tag{9}$$

Psychophysical experiments show that frequency bandwidths of simple cells in the visual cortex are one octave apart [5], for this reason we set $B_u = 1$. By setting the frequency cut-off to $-6$ dB, we determined the next ratio:

$$\alpha = \frac{0.56}{u} \tag{10}$$

The following values of radial frequency were used: $u = \left\{2\sqrt{2}, 4\sqrt{2}, 8\sqrt{2}, 16\sqrt{2}, 32\sqrt{2}, 64\sqrt{2}\right\}$ cycles/image-width for an image of size $256 \times 256$.

The last setting guarantees that the passband filter with the highest radial frequency falls inside the image array. At this point, we rule out low-pass filter and filters with low radial frequencies because these filters capture spatial variations that are too large for textures [14].

In order to determine the number of orientations, we use isotropic Gabor filters. In this case, $\alpha = \beta = 1$ and $B_\theta$ can be determined using:

$$\beta = \frac{\sqrt{\log(2)}}{\sqrt{2}\pi u \tan\left(\frac{B_\theta}{2}\right)} \tag{11}$$

In this way, $B_\theta = 37°$ is obtained, but for computational efficiency we set $B_\theta = 30°$.

### B. Feature extraction

Each filtered image, $f_i$, is subject to a sigmoid transformation that can be interpreted as a blob detector. Jain used an empirical value of $\gamma = 0.25$. We reached best performance using $\gamma = 0.1$.

$$\phi(f_i) = \tanh(\gamma f_i) = \frac{1 - e^{-2\gamma f_i}}{1 + e^{-2\gamma f_i}} \tag{12}$$

### C. Smoothing

Jain [1] also suggested to apply a Gaussian window function to each filtered image. The bandwidth of each Gaussian function is proportional to the average size of intensity variations in the image.

### D. Clustering

The last part of the algorithm consists in integrating features corresponding to different filters to produce a good segmentation. If feature vectors are capable of discriminating patterns belonging to different textures, each category will form a cluster. The clustering algorithm used in [1] is K-means with initial random seeds.

The issue of clustering or grouping $n$ objects into $K$ groups arises in many scientific disciplines and is not always easy to obtain an optimal partition. K-means is a very popular algorithm. However, the algorithm is prone to the initializing values which greatly influence the determination of an optimal solution. Here, we used an initialization procedure proposed in [15]. Bradley suggested using a bootstrap type procedure for finding seeds. Several different subsamples of dataset are each clustered using K-means. Each clustering produces a different set of candidates from which the initializers are chosen.

## V. Experiments

The algorithm described above was tested with textured images extracted from the Brodatz album [16]. We used both Gabor and log-Gabor decomposition into the pipeline in order to demonstrate their performance. Several image mosaics were considered using between two up to five textures, (see Figure 6).

Feature vectors were built using 36 filters in each case. Furthermore, we included the spatial coordinates of the pixels, the mean, and the variance as additional features. Figure 7 illustrates the results for segmentation test.

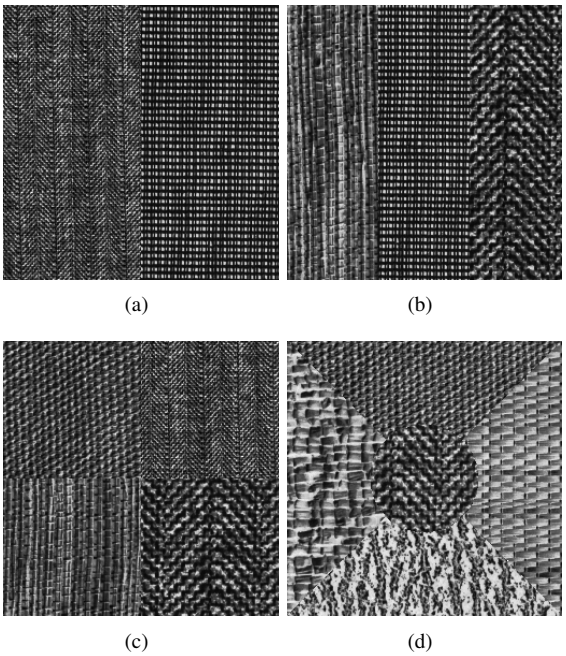


Figure 6. Brodatz texture images for segmentation. (a) D16 and D21 (left to right). (b) D79, D21 and D17 (left to right). (c) In clockwise direction D77, D16, D17, and D79. (d) D55, D77, D84, D24 and D17.

After segmentation tests, we evaluated them using confusion matrices and the accuracy rate (AR) was calculated using the next equation:

$$AR = \left( \frac{\sum_{i}^{k} a_{i,i}}{\sum_{i,j}^{k} a_{i,j}} \right) 100\% \tag{13}$$

where $(i, j)$ are matrix indexes and $k$ is the number of textures in the image.

Test accuracy is shown in Figure 8. Note that in all cases log-Gabor wavelets outperforms the Gabor wavelet. One can observe that as increasing the number of classes, decreases the accuracy of segmentation.

Due to space limitations, we only show the confusion matrices for the case of five textures, Table I shows the result for the segmentation with Gabor wavelets. Table II shows the segmentation result using log-Gabor wavelets.

## VI. Summary and conclusions

The main goal of this paper was to compare two Gabor schemes under the same conditions using a segmentation algorithm because Gabor filters have good performance in this issue. We selected the optimal parameters for Gabor filters and we tried to keep the equivalent values in the log-Gabor scheme. Although Jain's algorithm is already proven, we modified some stages by adding an initialization of centroids. Based on

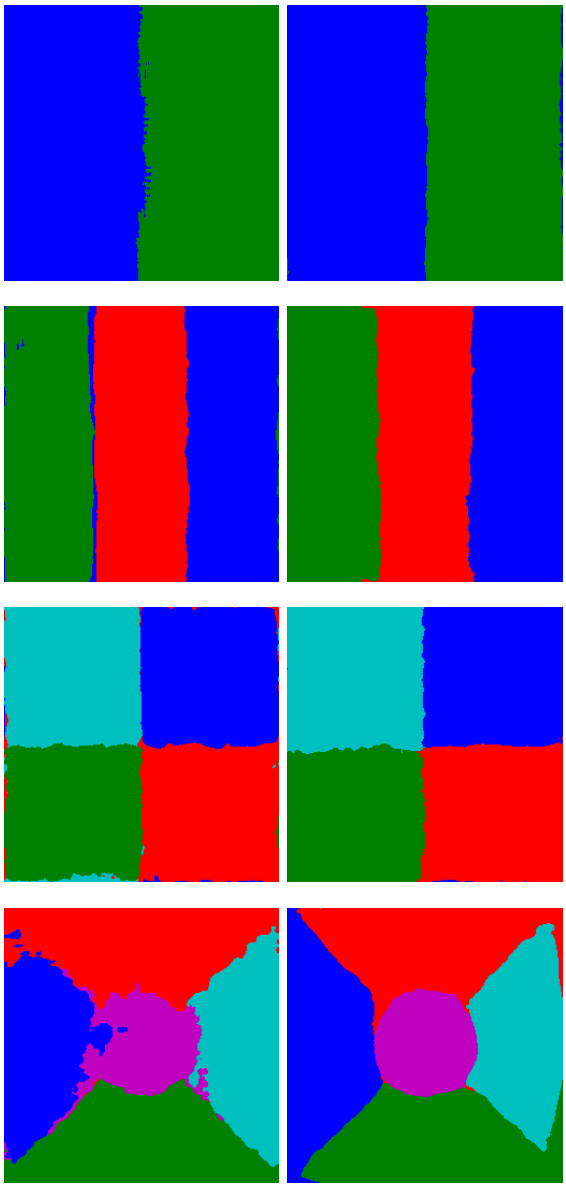

(a) (b)

Figure 7. Segmentation obtained using a total of 36 filters, pixel coordinates, mean, and variance. (a) Gabor wavelets segmentation. (b) Log-Gabor wavelet results.

Table I
CONFUSION MATRIX FOR THE EXPERIMENT WITH FIVE TEXTURES AND GABOR FILTERS AS A DECOMPOSITION SCHEME. IN THIS EXPERIMENT THE GAP BETWEEN GABOR AND LOG-GABOR WAVELETS IS WIDER. NEVERTHELESS, WE OBTAINED AN AR = 91.48%, WHICH IS BETTER THAN JAIN'S ALGORITHM. IN [1], THEY REPORTED 80% OF PIXELS CORRECTLY SEGMENTED.

| | | Predicted | | | | |
|---|---|---|---|---|---|---|
| | | 1 | 2 | 3 | 4 | 5 |
| Actual | 1 | 11895 | 1167 | 0 | 561 | 757 |
| | 2 | 0 | 14164 | 0 | 0 | 126 |
| | 3 | 0 | 736 | 12385 | 613 | 666 |
| | 4 | 0 | 0 | 0 | 14496 | 0 |
| | 5 | 498 | 131 | 0 | 327 | 7014 |

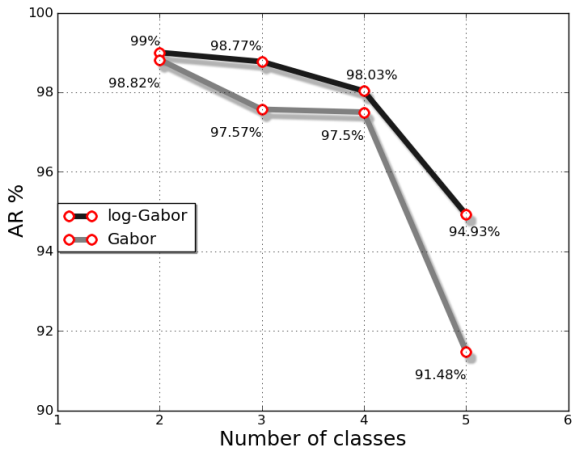


Figure 8. This plot represents the number of classes versus AR. As you can see, in the case of two textures, both Gabor and log-Gabor filters have almost the same performance but by increasing the number of classes, Gabor filters make more mistakes which leads us think that in case of more complex patterns log-Gabor filters can do better segmentation with fewer errors

Table II
CONFUSION MATRIX FOR THE EXPERIMENT WITH FIVE TEXTURES AND LOG-GABOR FILTERS AS A DECOMPOSITION SCHEME. IN THIS EXPERIMENT WE OBTAINED AN AR INDEX OF 94.93% PIXELS CORRECTLY CLASSIFIED. THIS RATIO OUTPERFORMS GABOR SCHEME RESULT.

| | | Predicted | | | | |
|---|---|---|---|---|---|---|
| | | 1 | 2 | 3 | 4 | 5 |
| Actual | 1 | 14106 | 242 | 0 | 32 | 0 |
| | 2 | 108 | 13810 | 224 | 0 | 148 |
| | 3 | 0 | 501 | 12510 | 1384 | 5 |
| | 4 | 209 | 9 | 0 | 14262 | 16 |
| | 5 | 110 | 99 | 81 | 156 | 7524 |

biological studies we considered six scales and six orientations (Jain used only 4 filters). Results show that log-Gabor outperforms Gabor filters in complex textures. For the test of five textures log-Gabor provides 94.92% of accuracy while Gabor scheme scored 91.48% of pixels correctly classified. Both schemes outperform Jain's report. Major differences occur at the borders between textures. Confusion matrices, in Table I and Table II, show that major mistakes are between textures D55 and D77 for Gabor scheme and between D77 and D84 for log-Gabor scheme.

## ACKNOWLEDGMENTS

This work has been supported by the following UNAM grants PAPIIT IN113611 and IXTLI IX100610 and by the Spanish Ministry of Science and Technology under projects TEC2010-20307 and TEC2010-09834-E.

## REFERENCES

[1] A. K. Jain and F. Farrokhnia, "Unsupervised texture segmentation using Gabor filters," *Pattern Recognition.*, vol. 24, pp. 1167–1186, 1991.
[2] D. H. Hubel and T. N. Wiesel, *Brain and Visual Perception: The Story of a 25-year Collaboration*. New York: Oxford University Press., 2005.
[3] D. J. Field, "Relations between the statistics of natural images and the response properties of cortical cells," *J. Opt. Soc. Am. A*, vol. 4, no. 12, pp. 2379–2394, 1987.

[4] D. Gabor, "Theory of communication," *J. Inst. Elec. Eng. (London)*, vol. 93III, pp. 429–457, 1946.
[5] J. G. Daugman, "Uncertainty relation for resolution in space, spatial frequency, and orientation optimized by two-dimensional visual cortical filters," *J. Opt. Soc. Am. A*, vol. 2, pp. 1160–1169, 1985.
[6] A. Kong, "An analysis of Gabor detection," in *Image Analysis and Recognition*, ser. Lecture Notes in Computer Science, M. Kamel and A. Campilho, Eds. Springer Berlin / Heidelberg, 2009, vol. 5627, pp. 64–72.
[7] R. Redondo, F. Šroubek, S. Fischer, and G. Cristóbal, "Multifocus image fusion using the log-Gabor transform and a multisize windows technique," *Information Fusion*, vol. 10, no. 2, pp. 163–171, 2009.
[8] A. C. Bovik, M. Clark, and W. S. Geisler, "Multichannel texture analysis using localized spatial filters," *IEEE Transactions on Pattern Analysis and Machine Intelligence*, vol. 12, pp. 55–73, 1990.
[9] R. Sandler and M. Lindenbaum, "Optimizing gabor filter design for texture edge detection and classification," *Int. J. Comput. Vision*, vol. 84, no. 3, pp. 308–324, September 2009.
[10] D. Dunn, W. E. Higgins, and J. Wakeley, "Texture segmentation using 2-d Gabor elementary functions," *IEEE Transactions on Pattern Analysis and Machine Intelligence*, vol. 16, pp. 130–149, 1994.
[11] L.-L. SHEN and Z. JI, "Gabor wavelet selection and svm classification for object recognition," *Acta Automatica Sinica*, vol. 35, no. 4, pp. 350–355, 2009.
[12] S. Fischer, F. Šroubek, L. Perrinet, R. Redondo, and G. Cristóbal, "Self-invertible 2d log-Gabor wavelets," *Int. J. Comput. Vision*, vol. 75, no. 2, pp. 231–246, 2007.
[13] W. Wang, J. Li, F. Huang, and H. Feng, "Design and implementation of log-gabor filter in fingerprint image enhancement," *Pattern Recogn. Lett.*, vol. 29, pp. 301–308, February 2008.
[14] D. A. Clausi and M. E. Jernigan, "Designing Gabor filters for optimal texture separability," *Pattern Recognition*, vol. 33, no. 11, pp. 1835–1849, 2000.
[15] P. S. Bradley and U. M. Fayyad, "Refining initial points for k-means clustering," in *Proceedings of the Fifteenth International Conference on Machine Learning*. San Francisco, CA, USA: Morgan Kaufmann Publishers Inc., 1998, pp. 91–99.
[16] P. Brodatz, *Textures; a photographic album for artists and designers*. Dover Publications New York, 1966.